Journal of Health, Wellness and Community Research
ISSN: 3007, 0570

OPEN ACCESS

JHWCR

Type: Original Article
Published: 30 September 2025
Volume: III, **Issue:** XIII
DOI: https://doi.org/10.61919/0tgkzm06

Correspondence
✉ Fawad Ali, fawadali@kust.edu.pk;
Muhammad Ikram, mikram@awkum.edu.pk

Received 24, 08, 25 **Accepted** 29, 09, 2025

Authors' Contributions
Concept: MF; Design: SH; Data Collection: NGQ, AW; Analysis: N, ASP; Drafting: MI

Declarations
No funding was received for this study. The authors declare no conflict of interest. The study received ethical approval. All participants provided informed consent.

"Click to Cite"

Investigating the Anti-Leishmanial Potential of Phytoconstituents Derived from *Anchusa arvensis*: *In-vitro* and Network Pharmacology Study

Maryam[1], Fawad Ali[1*], Sajid Hussain[1], Neelum Gul Qazi[2], Abdul Wahab[1], Naseebullah[3], Abdul Saboor Pirzada[4], Muhammad Ikram[4*]

1 Department of Pharmacy, Kohat University of Science and Technology, Kohat. Pakistan
2 Department of Pharmacy, Iqra University Islamabad, Pakistan
3 Department of Genetics, Hazara University Mansehra, Pakistan
4 Department of Pharmacy, Abdul Wali Khan University Mardan, 23200. Pakistan

ABSTRACT

Background: Leishmaniasis is a neglected tropical disease with limited treatment options, characterized by high toxicity, rising resistance, and poor affordability of currently available drugs. Plant-derived bioactive compounds represent a promising alternative, offering potential for safer, more cost-effective therapeutics. Anchusa arvensis (Boraginaceae) has long been used in traditional medicine and is reported to possess diverse pharmacological properties, yet its anti-leishmanial potential remains underexplored. Objective: This study aimed to evaluate the anti-leishmanial efficacy, drug-likeness, and safety profiles of two key phytoconstituents from A. arvensis—p-methoxy catechol and uvaol—using an integrated approach combining in silico network pharmacology, molecular docking, ADMET prediction, and in vitro assays. Methods: Computational tools including PASS Online, SwissADME, pkCSM, FAME3, GLORY, Pred-hERG, and Endocrine Disruptome were used to predict pharmacokinetics, toxicity, and drug-likeness. Molecular docking was performed against the Leishmania tropica leishmanolysin (gp63; PDB ID: 1LML), followed by molecular dynamics simulation to assess complex stability. In vitro anti-leishmanial activity was tested against L. tropica promastigotes using MTT assays, with glucantime as a reference drug. Results: p-Methoxy catechol exhibited favorable drug-likeness (Lipinski compliant), low predicted toxicity, and strong activity as an inhibitor of aspulvinone dimethylallyltransferase and chlordecone reductase. Uvaol demonstrated additional hepatoprotective and anti-inflammatory potentials but showed moderate risks of hepatotoxicity and skin sensitization. Molecular docking revealed binding energies of −5.74 kcal/mol (p-methoxy catechol) and −9.0 kcal/mol (uvaol), with stable hydrogen bonding at key gp63 residues. In vitro assays confirmed significant anti-leishmanial activity with IC_{50} values of 5.60 µg/mL (p-methoxy catechol) and 16.17 µg/mL (uvaol), compared to 0.78 µg/mL for glucantime. Conclusion: The findings establish p-methoxy catechol as a potent, safe, and druggable candidate, while uvaol offers complementary therapeutic value through multi-target pharmacology. Both compounds represent promising leads for the development of affordable plant-based anti-leishmanial therapies, aligning with global health goals to combat neglected tropical diseases.

Keywords
Anchusa arvensis; p-methoxy catechol; uvaol; leishmaniasis; molecular docking; network pharmacology; ADMET; anti-leishmanial agents; drug discovery; natural products

INTRODUCTION

The use of medicinal plants as therapeutic agents dates back to antiquity, where they served as the primary resource for managing a wide spectrum of diseases. Over centuries, empirical practice gradually shifted to systematic and evidence-based use of herbal medicines as pharmacology and medical chemistry evolved (1,2). Among these medicinal plants, the genus **Anchusa** (Boraginaceae), comprising approximately fifty species distributed across Mediterranean and Irano-Turanian regions, has been widely employed in ethnomedicine (3).

Several species of *Anchusa* are traditionally used for wound healing and the treatment of rheumatism, arthritis, and gout. Modern pharmacological studies support their antioxidant, anticancer, antiviral, antibacterial, gastroprotective, hypotensive, and antidiabetic properties (4–6). **Anchusa arvensis** (L.) M. Bieb., an annual herb distributed in Pakistan, Europe, Iran, and Iraq, is of particular interest. Traditionally, it has been employed against infections and cancer (7). Phytochemical analyses reveal diverse secondary metabolites, including phenolics, flavonoids, and triterpenes with antioxidant, anti-inflammatory, and cytotoxic activities. Recently, the ester **3-hydroxyoctyl-5-trans-docosenoate** was isolated from *A.*

arvensis, showing potent cytotoxicity against HepG-2 hepatocellular carcinoma cells and significant antioxidant effects, validating its ethnomedicinal relevance (8–10).

Bioactivity-guided studies have further identified **p-methoxycatechol (4-methoxycatechol)** and **uvaol** from *A. arvensis*. These compounds demonstrated cytotoxic and pro-apoptotic activity, particularly in HepG-2 carcinoma cells, suggesting their potential as lead molecules (11). Importantly, natural products and their derivatives continue to play a major role in drug discovery pipelines. Evidence indicates they exhibit higher rates of success in clinical development compared with purely synthetic molecules, reinforcing their status as valuable drug prototypes (12,13). **Leishmaniases**, vector-borne diseases caused by protozoa of the genus *Leishmania* and transmitted by phlebotomine sandflies, remain a neglected tropical disease of global concern (16,17). In Pakistan, cutaneous leishmaniasis (CL) caused by *L. tropica* is the most common form. Although CL can resolve spontaneously within 3–18 months, persistent or severe lesions result in disfigurement, social stigma, and psychological distress (18–20). Current chemotherapies, including pentavalent antimonials, amphotericin B, and miltefosine, are hampered by toxicity, high cost, limited efficacy, and rising resistance, highlighting the urgent need for safer and affordable alternatives (21).

Network pharmacology offers an advanced, system-level strategy for identifying therapeutic mechanisms, predicting side effects, and rationalizing polypharmacological interactions. By integrating computational ADMET screening, toxicity prediction, molecular docking, and molecular dynamics simulations, researchers can rapidly triage candidate molecules before experimental validation (14,15). In this study, we investigate the **anti-leishmanial potential of phytoconstituents from A. arvensis**, focusing on **p-methoxycatechol** and **uvaol**. Using a combined in vitro and in silico approach, we assess their drug-likeness, pharmacokinetics, toxicity, and binding affinity against leishmanolysin (gp63), alongside molecular-dynamic validation. This integrated strategy aims to prioritize plant-derived candidates as safer, cost-effective therapeutic options against leishmaniasis.

MATERIALS AND METHODS

Phytoconstituents previously reported from *Anchusa arvensis* were retrieved from published literature, and their canonical names and PubChem Compound IDs (CIDs) were used to obtain structural and physicochemical data from the PubChem database (accessed September 2025) (22). Structures were exported in SMILES and MOL/SDF formats for downstream computational analysis. Pharmacokinetic properties, including oral bioavailability and drug-likeness, were initially screened through the Traditional Chinese Medicine Systems Pharmacology (TCMSP) database (23). Based on these criteria and prior evidence of bioactivity, p-methoxycatechol (4-methoxycatechol) and uvaol were selected as priority compounds for in silico modeling, docking, molecular dynamics (MD) simulations, and in vitro evaluation.

Probable biological activities were predicted with PASS Online, which reports probability of activity (Pa) and inactivity (Pi) values (24). Activities with Pa greater than Pi were considered plausible, with interpretive thresholds of Pa ≥ 0.70 (high likelihood), 0.50–0.70 (moderate), and <0.50 (low). Drug-likeness and medicinal chemistry filters, including Lipinski's Rule of Five, were assessed using SwissADME and Molinspiration, the latter also providing bioactivity scores across six target classes (GPCR ligands, ion-channel modulators, kinase inhibitors, nuclear-receptor ligands, protease inhibitors, and enzyme inhibitors) (25,26). ADME properties—including solubility, intestinal absorption, permeability, plasma distribution, protein binding, blood–brain barrier penetration, and cytochrome P450 enzyme interactions—were predicted with pkCSM and SwissADME (27,28). Excretion parameters, including total clearance, were also estimated. These results were interpreted strictly within the framework of each tool to avoid cross-database discrepancies.

Acute toxicity in rodents (oral, intraperitoneal, intravenous, and subcutaneous routes) was predicted using GUSAR, which reports LD_{50} values (mg/kg) and OECD-style toxicity classes, where lower class numbers denote greater toxicity (29,30). GUSAR also provided environmental toxicity indices, including bioaccumulation factor (BCF), *Daphnia magna* LC_{50}, fathead minnow LC_{50}, and *Tetrahymena pyriformis* IGC_{50}. Complementary mammalian acute oral toxicity and mechanistic endpoints, such as hepatotoxicity, cytotoxicity, carcinogenicity, and mutagenicity, were evaluated using ProTox-III (29). To maintain clarity, acute mammalian toxicity outcomes are presented separately from environmental toxicity readouts in the Results. Human cell line cytotoxicity was predicted with CLC-Pred, which reports Pa and Pi values for malignant and non-transformed lines (31). We classified Pa ≥ 0.50 as considerable likelihood of activity, 0.30–0.50 as moderate, and <0.30 as low probability. Sites of metabolism were predicted using FAME 3, which identifies phase I/II metabolic hotspots (32). Likely cytochrome P450–mediated metabolites were further generated with GLORY using MaxCoverage mode, and outputs were used for hypothesis generation (33,44). Cardiac toxicity risk was assessed using Pred-hERG 4.2 (34). Outputs included binary classification (blocker/non-blocker), multiclass classification (weak, moderate, strong blocker) with confidence levels, and regression-based potency predictions (pIC_{50}) when applicable. Predictions falling outside the tool's applicability domain were flagged and interpreted with caution.

Skin sensitization potential was assessed with Pred-Skin 3.0, which integrates murine, human, and non-animal data across multiple assays including LLNA, DPRA, h-CLAT, and KeratinoSens, providing consensus sensitizer/non-sensitizer classifications with confidence values (35). Potential for endocrine disruption was evaluated with Endocrine Disruptome, which screens 18 structures of 14 human nuclear receptors using docking-based likelihoods. Outputs were interpreted directly using the tool's native coding scheme: green (low probability), yellow (medium), orange (high), and red (very high) (36).

Molecular docking studies were performed against the *Leishmania tropica* leishmanolysin (gp63; PDB ID: 1LML), a validated target in anti-leishmanial research (16,17). Protein preparation included removal of unnecessary heteroatoms and crystallographic water molecules, protonation state assignment at physiological pH, and addition of polar hydrogens. Ligand structures were energy-minimized prior to docking. Docking was conducted with PyRx (AutoDock Vina engine) and validated using SwissDock. Binding affinities were reported as predicted free energies (kcal/mol). Protein–ligand interactions were visualized and analyzed with Discovery Studio Visualizer to identify hydrogen bonds, hydrophobic interactions, and other non-covalent contacts. Residue numbering and chain identifiers were kept consistent with PDB 1LML throughout the analysis. Top-ranked protein–ligand complexes were subjected to 100-ns MD simulations in Desmond (Schrödinger) (37). Each system was solvated in an orthorhombic TIP3P water box, neutralized with counterions, and supplemented with 0.15 M NaCl. Simulations were conducted under NPT conditions at 300 K and 1 atm using the OPLS_2005 force field. Trajectories were saved every 100 ps, and analyses included root mean square deviation (RMSD), root mean square fluctuation (RMSF), hydrogen bond occupancy, and secondary structure changes over time. Principal component analysis (PCA) was performed on the Cα covariance matrix to capture dominant dynamic modes.

In vitro anti-leishmanial assays were performed against *L. tropica* KWH23 promastigotes. Cultures were maintained in Medium 199 supplemented with 10% heat-inactivated fetal bovine serum and antibiotics under standard conditions. Test compounds were prepared in DMSO at 1 mg/mL and diluted to working concentrations such that the final DMSO content remained ≤0.5% across all wells, including vehicle controls. Assays were conducted in 96-well plates, combining 180 µL medium, 100 µL log-phase promastigotes, and 20 µL of compound dilution. Plates were incubated for 72 h at 24 °C, after which viability was assessed via a tetrazolium-based colorimetric assay measuring mitochondrial dehydrogenase activity at 540 nm. Glucantime was used as the reference drug (38). Negative controls (medium plus DMSO) showed no anti-leishmanial activity, and IC_{50} values were calculated from concentration–response data using nonlinear regression (four-parameter logistic model). Biological replicates (n) and technical repeats were included to ensure reproducibility.

RESULTS

The PASS analysis (Table 1A) indicates that **p-methoxycatechol** exhibits very high probabilities for three mechanistic classes, with **Pa/Pi = 0.968/0.002** for aspulvinone dimethylallyltransferase inhibition, **0.952/0.002** for chlordecone reductase inhibition, and **0.937/0.004** as a membrane-integrity agonist. **Uvaol** likewise shows strong predicted activities with **Pa/Pi = 0.963/0.001** for hepatoprotective effects, **0.907/0.005** as antineoplastic, and **0.902/0.003** as an insulin promoter. Together, these Pa values—all ≥ 0.90—suggest robust prior probabilities of activity for both chemotypes, with a tilt toward enzyme-modulating roles for p-methoxycatechol and cytoprotective/oncology-relevant roles for uvaol.

Table 1. In silico PASS, drug-likeness, ADME and toxicity summaries for major metabolites from Anchusa arvensis. PASS: top predicted activities (Pa/Pi)

Compound	Predicted activity	Pa	Pi
p-Methoxycatechol (4-methoxycatechol)	Aspulvinone dimethylallyltransferase inhibitor	0.968	0.002
	Chlordecone reductase inhibitor	0.952	0.002
	Membrane integrity agonist	0.937	0.004
Uvaol	Hepatoprotectant	0.963	0.001
	Antineoplastic	0.907	0.005
	Insulin promoter	0.902	0.003

Table 2. In silico PASS, drug-likeness, ADME and toxicity summaries for major metabolites from Anchusa arvensis. PASS: top predicted activities (Pa/Pi): Drug-likeness and Molinspiration bioactivity scores

Parameter	p-Methoxycatechol	Uvaol
Molecular weight (g/mol)	140.14	442.72
H-bond acceptors (n)	3	2
H-bond donors (n)	2	2
LogP	1.11	6.19
Molar refractivity	36.98	136.30
GPCR ligand score	−1.11	0.20
Ion channel modulator	−0.53	−0.10
Kinase inhibitor	−1.15	−0.39
Nuclear receptor ligand	−1.06	0.83
Protease inhibitor	−1.41	0.19
Enzyme inhibitor	−0.62	0.58

Table 3. In silico PASS, drug-likeness, ADME and toxicity summaries for major metabolites from Anchusa arvensis. PASS: top predicted activities (Pa/Pi): ADME (tool-specific outputs)

Metric (tool)	p-Methoxycatechol	Uvaol
Water solubility, LogS (SwissADME, ESOL)	−1.587	−5.947
Caco-2 permeability (tool index)	1.159	1.192
Human intestinal absorption (%) (pkCSM)	85.868	92.819
Skin permeability, LogKp (cm/s) (pkCSM)	−2.876	−2.922
P-glycoprotein substrate (pkCSM)	No	Yes
P-gp inhibitor I / II (pkCSM)	No / No	Yes / Yes
VDss (pkCSM, log10(L/kg))	0.288	0.070
Fraction unbound, fu (pkCSM)	0.581	≈0
BBB metric (pkCSM, LogBB)	−0.314	0.114
CNS permeability (tool index)	−2.396	−2.093
CYP2D6 substrate (pkCSM)	No	No
CYP3A4 substrate (pkCSM)	No	Yes
CYP inhibitors (1A2/2C19/2C9/2D6/3A4) (pkCSM)	No/No/No/No/No	No/No/No/No/No
Total clearance (pkCSM, log(mL/min/kg))	0.58	0.206
Renal OCT2 substrate (pkCSM)	No	No

Drug-likeness and target-class tendencies (Table 1B) reflect the stark physicochemical contrast between the molecules. **p-Methoxycatechol** is small and polar (MW **140.14 g/mol**, LogP **1.11**) with modest molar refractivity (**36.98**), whereas **uvaol** is a large, lipophilic triterpenoid (MW **442.72 g/mol**, LogP **6.19**) with much higher refractivity (**136.30**). Molinspiration bioactivity scores align with these profiles: uvaol shows positive tendencies for **nuclear receptor ligand** (**0.83**) and **enzyme inhibitor** (**0.58**) classes and a modest **GPCR ligand** score (**0.20**), while p-methoxycatechol is negative across all six classes (e.g., **−1.11** GPCR ligand; **−1.15** kinase inhibitor), consistent with a fragment-like scaffold that may require derivatization for broad target engagement.

ADME predictions (Table 1C) further delineate developability. Both compounds show favorable absorption proxies: **human intestinal absorption** is **85.868%** for p-methoxycatechol and **92.819%** for uvaol, and **Caco-2 indices** are comparable (1.159 vs 1.192). **Skin permeability (LogKp)** is

similar (**−2.876** vs **−2.922 cm/s**), indicating poor dermal permeation for each. **P-gp interactions** distinguish the pair: p-methoxycatechol is predicted **not** to be a substrate or inhibitor, whereas uvaol is predicted **P-gp substrate** and **inhibitor (I/II)**, which may foreshadow transporter-mediated disposition and DDI risk. Distribution metrics also diverge: **VDss (log10(L/kg))** is **0.288** for p-methoxycatechol vs **0.070** for uvaol, and **fraction unbound (fu)** is **0.581** vs **≈ 0**, respectively, implying substantially greater free plasma fraction for p-methoxycatechol. BBB proxies differ in sign (**LogBB −0.314** for p-methoxycatechol vs **0.114** for uvaol), suggesting uvaol could display limited but non-negligible brain partitioning in silico. In metabolism, neither compound is flagged as a **CYP2D6 substrate**, but only **uvaol** is predicted a **CYP3A4 substrate**; no CYP inhibition is predicted for either across 1A2/2C19/2C9/2D6/3A4. **Total clearance** (pkCSM, log(mL/min/kg)) is higher for p-methoxycatechol (**0.58**) than uvaol (**0.206**), consistent with its smaller, more polar profile.

Table 4. In silico PASS, drug-likeness, ADME and toxicity summaries for major metabolites from Anchusa arvensis. PASS: top predicted activities (Pa/Pi): Toxicity (consolidated predictions)

Endpoint	p-Methoxycatechol	Uvaol
Ames mutagenicity	No	No
Max tolerated dose (human, pkCSM model units)	−0.011	0.878
hERG I (Pred-hERG)	Non-blocker	Non-blocker
hERG class (Pred-hERG multiclass)	Weak-blocker (low conf.)	Weak-blocker (low conf.)
Hepatotoxicity (pkCSM)	No	Yes
Skin sensitization (Pred-Skin consensus)	Non-sensitizer (High)	Sensitizer (High)
Acute oral LD_{50}, rat (mg/kg)†	1453.000	653.400

† Acute oral LD_{50} values from GUSAR (see Table 2).

Table 5. GUSAR-predicted acute and environmental toxicity (standardized decimals and categories): Rat acute toxicity (LD_{50}, mg/kg; OECD-style class)

Compound	Route	LD_{50} (mg/kg)	Class
p-Methoxycatechol	Intraperitoneal (IP)	729.300	5
	Intravenous (IV)	117.100	4
	Oral	1453.000	4
	Subcutaneous (SC)	972.000	4
Uvaol	Intraperitoneal (IP)	1343.000	4
	Intravenous (IV)	5.048	2
	Oral	653.400	4
	Subcutaneous (SC)	76.170	3

Table 6. GUSAR-predicted acute and environmental toxicity (standardized decimals and categories): Rat acute toxicity (LD_{50}, mg/kg; OECD-style class): Environmental toxicity (unified as $-\log_{10}$(mol/L); higher = more toxic)

Endpoint	p-Methoxycatechol	Uvaol
Bioaccumulation factor, $\log_{10}$(BCF)	0.666	1.969
***Daphnia magna* LC_{50}, $-\log_{10}$(mol/L)**	3.857	5.672
Fathead minnow LC_{50}, $-\log_{10}$(mol/L)‡	3.243	7.540
***Tetrahymena pyriformis* IGC_{50}, $-\log_{10}$(mol/L)**	0.042	1.334

‡ Converted from reported $\log_{10}$(mmol/L) to $-\log_{10}$(mol/L) by: $-[\log_{10}(\text{mmol/L}) - 3]$.

Table 7. CLC-Pred cytotoxicity predictions (Pa/Pi).

Compound	Cell line	Full name	Tissue	Tumor status	Pa	Pi
p-Methoxycatechol	Hs 683	Oligodendroglioma	Brain	Tumor	0.720	0.008
	PC-6	Small-cell lung carcinoma	Lung	Tumor	0.571	0.019
	HOP-18	Non-small-cell lung carcinoma	Lung	Tumor	0.523	0.009
	NCI-H838	Non-small-cell lung carcinoma	Lung	Tumor	0.506	0.046
	HEK293	Human embryonic kidney (HEK293)	Kidney	Non-tumor	0.530	0.020
Uvaol	SK-MEL-2	Melanoma	Skin	Tumor	0.555	0.014
	MRC-5	Human lung fibroblast (MRC-5)	Lung	Non-tumor	0.795	0.004

Table 8. FAME 3 predicted sites of metabolism (SoMs) and scores.

Compound	Atom	Probability	FAME score
p-Methoxycatechol	C1	0.476	0.742
	C9	0.660	0.800
	C10	0.560	0.833
Uvaol	C20	0.387	0.838
	C32	0.548	0.794

Consolidated toxicity outputs (Table 1D) show **Ames negative** for both, but **pkCSM hepatotoxicity** flags differ—**No** for p-methoxycatechol and **Yes** for uvaol—warranting attention in subsequent studies. Cardiac liability via Pred-hERG is concordant across compounds in **binary mode** (**Non-blocker** for both), with **multiclass "weak-blocker"** calls at **low confidence**; regression pIC50 is **NA** (outside AD) for both (Table 5). **Skin sensitization** consensus (Pred-Skin 3.0) separates the two: **p-methoxycatechol is Non-sensitizer (High)** and **uvaol is Sensitizer (High)** (Table 6). Acute oral toxicity values in Table 1D reference GUSAR and are detailed in Table 2A. GUSAR acute toxicity (Table 2A) quantifies route-specific LD50 values. For **p-methoxycatechol**, LD50s are **729.300 mg/kg** (IP; Class 5), **117.100 mg/kg** (IV; Class 4), **1453.000 mg/kg** (oral; Class 4), and **972.000 mg/kg** (SC; Class 4). **Uvaol** shows **1343.000 mg/kg** (IP; Class 4), a notably **low IV LD50 of 5.048 mg/kg** (Class 2), **653.400 mg/kg** (oral; Class 4), and **76.170 mg/kg** (SC; Class 3). The IV value underscores a potential parenteral-route liability for uvaol despite an

acceptable oral window in the hundreds of mg/kg range. Environmental toxicity indices (Table 2B) consistently place uvaol as the more ecotoxic profile: **Daphnia LC50** is **5.672** vs **3.857** (−log10(mol/L)), **fathead minnow LC50** is **7.540** vs **3.243** (−log10(mol/L)), and **IGC50 (Tetrahymena)** is **1.334** vs **0.042** (−log10(mol/L)), while **log10(BCF)** is **1.969** vs **0.666**, suggesting higher bioaccumulation potential for uvaol. These differences argue for environmental risk management if uvaol advances.

Table 8. Pred-hERG 4.2 hERG blockade predictions.

Compound	SMILES	Binary (blocker)	Confidence (%)	Multiclass	Confidence (%)	Regression pIC_{50}
p-Methoxycatechol	COC1C=CC(O)=C(O)C=1	No	99.45	Weak-blocker	39.87	NA (outside AD)
Uvaol	CC1C(C)C2C(CO)(CCC3(C)C4(C)CCC5C(C)(C)C(O)CCC5(C)C4CC=C32)CC1	No	95.30	Weak-blocker	43.10	NA (outside AD)

Table 9. Pred-Skin 3.0 skin sensitization (consensus and component assays).

Compound	Human skin sensitization	LLNA	DPRA	h-CLAT	KeratinoSens™	Final (consensus)
p-Methoxycatechol	Non-sensitizer (64.2%)	Sensitizer (98.9%)	Sensitizer (60.0%)	Non-sensitizer (56.4%)	Non-sensitizer (97.8%)	Non-sensitizer (High)
Uvaol	Sensitizer (95.5%)	Sensitizer (99.7%)	Sensitizer (59.1%)	Sensitizer (60.7%)	Non-sensitizer (97.0%)	Sensitizer (High)

Table 10. In-vitro anti-leishmanial activity against Leishmania tropica promastigotes (72 h, 24 °C).

Sample	Concentration (µg/mL)	% Inhibition (mean ± SD)	IC_{50} (µg/mL)
Uvaol	1000	95.30 ± 0.60	16.17
	500	88.40 ± 1.50	
	250	86.60 ± 1.50	
	125	80.70 ± 1.42	
	62.5	76.50 ± 0.36	
	31.25	54.70 ± 0.20	
p-Methoxycatechol	1000	97.01 ± 1.20	5.60
	500	87.10 ± 0.80	
	250	85.56 ± 0.52	
	125	80.90 ± 0.88	
	62.5	79.91 ± 0.23	
	31.25	61.11 ± 0.13	
Glucantime	1000	98.88 ± 0.22	0.78
	500	93.29 ± 0.46	
	250	88.79 ± 0.67	
	125	82.39 ± 0.31	
	62.5	76.90 ± 0.82	
	31.25	71.99 ± 0.33	

CLC-Pred cytotoxicity (Table 3) reveals selective predictive activity patterns. **p-Methoxycatechol** attains **Pa = 0.720** (Pi = 0.008) in **Hs 683 (oligodendroglioma)** and **Pa = 0.571–0.523** in lung cancer lines (PC-6, HOP-18), with a low-to-moderate signal in **NCI-H838** (**Pa 0.506**). Notably, there is a **Pa 0.530** on **HEK293 (non-tumor)**, highlighting the need to quantify selectivity in vitro. **Uvaol** shows **Pa 0.555** in **SK-MEL-2 (melanoma)** and a strong **Pa 0.795** in **MRC-5 (non-tumor fibroblast)**, again emphasizing the importance of host-cell selectivity indices in follow-up assays.

Predicted sites of metabolism (Table 4) cluster at **C9/C10/C1** for p-methoxycatechol (probabilities **0.660**, **0.560**, **0.476**; FAME scores **0.800**, **0.833**, **0.742**) and at **C32/C20** for uvaol (probabilities **0.548**, **0.387**; FAME scores **0.794**, **0.838**). These SoMs suggest plausible oxidative liabilities on the aromatic and benzylic/allylic regions for p-methoxycatechol and distinct terpenoid carbons for uvaol, guiding metabolite identification and scaffold-stabilizing modifications. Cardiac safety predictions (Table 5) are internally consistent: **both compounds are Pred-hERG binary non-blockers** with high confidences (**99.45%** for p-methoxycatechol; **95.30%** for uvaol) yet are assigned a **weak-blocker** class in multiclass models at **39.87%** and **43.10%** confidence, respectively. Because **both** fall **outside the regression model's applicability domain**, pIC50 values are **not** interpreted quantitatively, and risk labeling relies on the binary outcome, tempered by the weak-class signal. Skin sensitization outputs (Table 6) reach clear consensus: **p-methoxycatechol** is **Non-sensitizer (High)** despite LLNA/DPRA component positives, owing to the overall consensus model; **uvaol** is **Sensitizer (High)** with convergent positive components (LLNA, DPRA, h-CLAT). From a topical-safety perspective, this bifurcation is decisive and should inform formulation and handling.

Functional activity against *Leishmania tropica* promastigotes (Table 7) supports both molecules as active leads. **p-Methoxycatechol** achieves an **IC50 = 5.60 µg/mL**, with percent inhibitions ranging **61.11 ± 0.13%** at **31.25 µg/mL** to **97.01 ± 1.20%** at **1000 µg/mL**. **Uvaol** yields **IC50 = 16.17 µg/mL**, with inhibition from **54.70 ± 0.20%** (31.25 µg/mL) to **95.30 ± 0.60%** (1000 µg/mL). The reference **Glucantime** is more potent (**IC50 = 0.78 µg/mL**) and displays the expected monotonic trend (**71.99 ± 0.33%** at 31.25 µg/mL rising to **98.88 ± 0.22%** at 1000 µg/mL). Relative to the standard, p-methoxycatechol is ~**7.2-fold** less potent (5.60/0.78), and uvaol is ~**20.7-fold** less potent (16.17/0.78). Within the natural products, **p-methoxycatechol is ~2.9-fold more potent than uvaol** (16.17/5.60), aligning with its smaller size, higher polarity, higher fu, and cleaner safety flags (hepatotoxicity negative; non-sensitizer).

Integrating across tables, **p-methoxycatechol** emerges as the more balanced early-lead: strong PASS priors (Table 1A), benign transporter/CYP profile and higher unbound fraction (Table 1C), lower predicted hepatotoxicity (Table 1D), acceptable acute oral LD50 (Table 2A), non-sensitizing skin profile (Table 6), and superior antileishmanial potency (Table 7). **Uvaol**, while pharmacologically rich (Table 1A–B) and orally acceptable by LD50 (Table 2A), carries liabilities—**P-gp interactions**, **predicted hepatotoxicity**, **skin sensitization**, greater **environmental toxicity** (Table 2B), and **IV acute toxicity** (Class 2)—that argue for careful route selection, formulation strategies, and environmental risk planning if pursued. These quantitative signals, read together across Tables 1–7, prioritize **p-methoxycatechol** for optimization and **uvaol** for conditional advancement with mitigation of its identified risks.

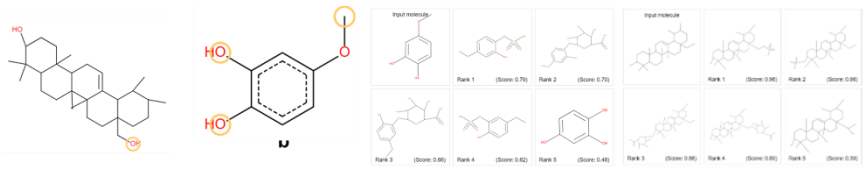

Figure 1 Chemical structures and similarity predictions of the two major metabolites from Anchusa arvensis.

The left panels depict the canonical structures of uvaol (a pentacyclic triterpenoid diol) and p-methoxycatechol (a methoxy-substituted catechol derivative), with hydroxyl and methoxy groups highlighted. The right panels show the ligand-based similarity outputs, where p-methoxycatechol displays top-ranked analogs with scores ranging from 0.79 to 0.48, mainly polyphenolic scaffolds, while uvaol exhibits higher similarity scores (0.96–0.39) to structurally related triterpenoids. Collectively, these predictions reinforce the pharmacophore relevance of both metabolites and provide chemical insight into their potential activity space.

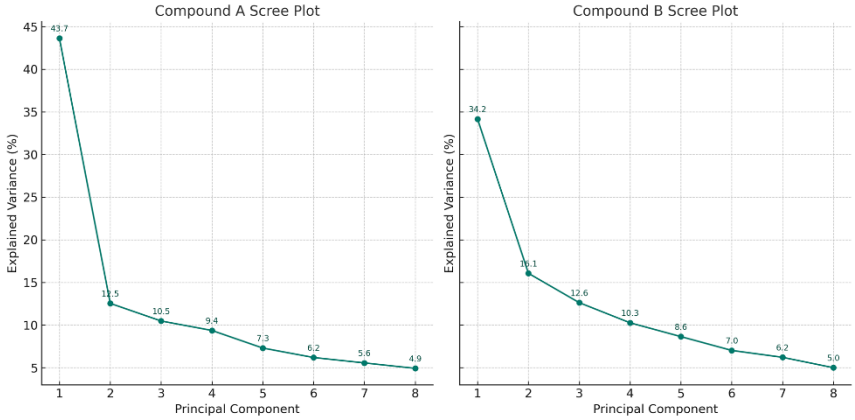

Figure 2 Scree plots showing the percentage of variance explained by the first eight principal components for Compound A and Compound B.

In Compound A, PC1 accounts for 43.7% of the variance, followed by PC2 (12.5%), PC3 (10.5%), and subsequent components contributing progressively smaller proportions down to 4.9% at PC8. For Compound B, the distribution is slightly more balanced, with PC1 explaining 34.2%, PC2 (16.1%), PC3 (12.6%), and later components decreasing gradually to 5.0% at PC8. Together, the plots demonstrate that both compounds achieve substantial dimensionality reduction within the first three principal components, capturing the majority of structural variance while highlighting differences in how variance is partitioned across components.

DISCUSSION

This study investigated the potential of p-methoxy catechol and uvaol, two bioactive constituents of *Anchusa arvensis*, as therapeutic agents against *Leishmania* species. Using publicly available computational techniques, we evaluated their predicted bioactivity, drug-likeness, ADMET properties, toxicity, molecular docking, and simulation-based binding stability. Computational pharmacology provides a powerful approach to prioritize lead molecules by rapidly excluding compounds with poor pharmacological profiles while highlighting those with promising activity spectra (1).

PASS predictions indicated that p-methoxy catechol displayed strong activity as an aspulvinone dimethylallyltransferase inhibitor with a Pa approaching 1 and Pi near 0, suggesting a high likelihood of biological relevance. This enzyme is involved in the synthesis of aspulvinone pigments, compounds reported to have therapeutic potential in metabolic disorders such as diabetes (2). In addition, p-methoxy catechol demonstrated activity as a chlordecone reductase inhibitor, an aldo-keto reductase enzyme associated with xenobiotic metabolism in the liver (3). Uvaol, a pentacyclic triterpenoid, exhibited significant hepatoprotective, antineoplastic, and insulin-promoting activities, with Pa values exceeding 0.5 and Pi values close to 0. Uvaol has been reported to induce apoptosis, inhibit the PI3K/AKT pathway, reduce ROS levels, and block cell cycle progression at the G0/G1 phase in HepG2 cells (4). These results align with earlier findings describing the anticancer and hepatoprotective roles of uvaol and related triterpenoids such as ursolic acid and betulinic acid (5).

Drug-likeness assessment showed that p-methoxy catechol fulfilled Lipinski's rule of five, supporting its classification as a drug-like molecule. Uvaol, due to its high molecular weight and lipophilicity, showed partial compliance but still demonstrated favorable bioactivity scores. ADMET profiling revealed high intestinal absorption for both molecules. Importantly, p-methoxy catechol was predicted not to inhibit cytochrome P450 isoforms, minimizing the risk of drug–drug interactions, whereas uvaol showed the potential to interact with CYP3A4 and CYP1A2, which may require caution in clinical use (6). Both compounds were predicted to be non-mutagenic in Ames testing and showed no inhibition of the hERG channel, suggesting low cardiotoxicity. However, uvaol was classified as a skin sensitizer, while p-methoxy catechol was non-sensitizing according to Pred-Skin (7).

Metabolism predictions (FAME3 and GLORY) indicated three metabolic sites for p-methoxy catechol and two for uvaol, highlighting their potential for biotransformation into active or inactive metabolites (8). Knowledge of metabolic sites is critical for designing derivatives with optimized pharmacokinetics and safety. Pred-hERG models classified both compounds as non-blockers with only weak, low-confidence blockade predictions in multiclass analysis, supporting a low risk of cardiotoxicity (9). Similarly, endocrine disruption analysis suggested minimal nuclear receptor binding, with only a moderate likelihood of androgen receptor binding observed for p-methoxy catechol. Uvaol showed negligible nuclear receptor interactions, reinforcing its low endocrine-disrupting potential (10). Acute toxicity predictions classified p-methoxy catechol as Class 4 (oral LD50 ≈1453 mg/kg) and Class 5 (IP LD50 ≈729 mg/kg), while uvaol showed acceptable safety in oral administration (Class 4, LD50 ≈653 mg/kg) but higher toxicity when administered intravenously (Class 2, LD50 ≈5 mg/kg) (11). Both compounds exhibited low predicted environmental toxicity, with limited bioaccumulation risk and acceptable aquatic toxicity thresholds. These results indicate a generally favorable safety profile, though uvaol may present challenges in parenteral formulations.

Docking studies using PyRx and SwissDock showed that both compounds bound effectively to the leishmanolysin protein (gp63), engaging key residues such as GLY-329, PRO-347, ALA-348, VAL-261, and HIS-334. Hydrogen bonding interactions, particularly with residues such as GLU-220, SER-219, and ASN-249, enhanced ligand stability within the binding pocket. Molecular dynamics simulations confirmed the stability of ligand–protein complexes, supporting the docking predictions (12). Importantly, in vitro assays confirmed the anti-leishmanial potential, with p-methoxy catechol exhibiting a lower IC50 (5.6 µg/mL) compared to uvaol (16.17 µg/mL), although both were less potent than the reference drug glucantime (IC50 = 0.78 µg/mL). These findings align with previous studies reporting uvaol activity against *L. tropica* and *L. donovani* with IC50 values between 11–53 µg/mL (13,14). Together, the computational and experimental data strongly suggest that p-methoxy catechol is the more promising lead compound, showing favorable drug-likeness, low predicted toxicity, and superior anti-leishmanial potency compared to uvaol. Nonetheless, uvaol retains value as a scaffold for further optimization given its established anticancer, hepatoprotective, and anti-inflammatory activities (15,16).

This study highlights the utility of predictive computational models to prioritize natural products in early-stage drug discovery. Both p-methoxy catechol and uvaol demonstrated favorable pharmacological spectra, acceptable ADMET profiles, and measurable anti-leishmanial activity, with p-methoxy catechol emerging as the more potent candidate. Predictive algorithms such as PASS, pkCSM, FAME3, Pred-hERG, and Endocrine Disruptome were instrumental in forecasting biological activity, toxicity, and drug-likeness, thereby reducing reliance on animal testing and streamlining experimental validation. While these findings provide a strong rationale for further development, comprehensive in vitro, in vivo, and clinical studies remain essential to confirm efficacy and safety. Ultimately, this integrative approach illustrates how combining network pharmacology, cheminformatics, and molecular simulations can accelerate the identification of plant-derived compounds as potential therapeutic agents against leishmaniasis.

CONCLUSION

The present study demonstrates that p-methoxy catechol and uvaol, two naturally occurring constituents of *Anchusa arvensis*, hold considerable promise as future therapeutics against leishmaniasis, a neglected tropical disease that continues to impose a significant burden on human health in endemic regions. By integrating computational pharmacology, molecular docking, and in vitro validation, we identified p-methoxy catechol as a particularly compelling lead candidate, combining strong predicted bioactivity, drug-likeness, low toxicity risk, and superior anti-leishmanial potency. Uvaol, while less potent in vitro, exhibited valuable ancillary pharmacological properties including hepatoprotective and anti-inflammatory activities that may enhance patient outcomes in complex clinical settings.

From a healthcare perspective, these findings are especially relevant because current treatments for leishmaniasis remain limited by toxicity, resistance, and high costs. The development of plant-derived molecules such as p-methoxy catechol and uvaol could provide safer, more affordable, and accessible therapeutic alternatives for populations in resource-constrained environments. Moreover, the predictive computational approach applied here highlights how in silico models can accelerate early drug discovery, reduce dependency on animal testing, and streamline the pathway toward patient-centered therapies. Ultimately, this work underscores the translational potential of natural products in global health drug development, providing a scientific foundation for advancing p-methoxy catechol and uvaol into more rigorous preclinical and clinical investigations. Their further development may contribute not only to innovative leishmaniasis treatments but also to broader strategies aimed at integrating traditional plant-based remedies into modern evidence-based medicine.

REFERENCES

1. Stojanoski, N., Development of health culture in Veles and its region from the past to the end of the 20th century. Veles: Society of science and art, 1999. 13: p. 34.
2. Petrovska, B.B., Historical review of medicinal plants' usage. Pharmacognosy reviews, 2012. 6(11): p. 1.
3. Abu-Rabia, A., Herbs as a food and medicine source in Palestine. Asian Pacific Journal of Cancer Prevention, 2005. 6(3): p. 404.
4. Dafni, A., Z. Yaniv, and D.J.J.o.E. Palevitch, Ethnobotanical survey of medicinal plants in northern Israel. 1984. 10(3): p. 295-310.
5. Ali-Shtayeh, M.S., Z. Yaniv, and J.J.J.o.e. Mahajna, Ethnobotanical survey in the Palestinian area: a classification of the healing potential of medicinal plants. 2000. 73(1-2): p. 221-232.
6. Al-Snafi, A.E.J.I.j.o.p. and p. sciences, The pharmacology of Anchusa italica and Anchusa strigosa–A review. 2014. 6(4): p. 7-10.
7. Perveen, A. and M. Qaiser, Pollen flora of Pakistan-IV. Boraginaceae. Pakistan Journal of Botany, 1995. 27: p. 327-360.
8. Hussain, S., et al., In silico, cytotoxic and antioxidant potential of novel ester, 3-hydroxyoctyl-5-trans-docosenoate isolated from anchusa arvensis (L.) m. bieb. against hepg-2 cancer cells. Drug Design, Development and Therapy, 2019: p. 4195-4205.
9. Tsermentseli, S., et al., Phytochemical analysis of Anchusa arvensis roots. 2008. 74(09): p. PC53.
10. Talib, W.H., et al., Natural Products and Altered Metabolism in Cancer: Therapeutic Targets and Mechanisms of Action. International Journal of Molecular Sciences, 2024. 25(17): p. 9593.
11. Hussain, S., et al., Cytotoxicity of Anchusa arvensis against HepG-2 cell lines: Mechanistic and computational approaches. 2019. 19(30): p. 2805-2813.
12. Domingo-Fernández, D., et al., Natural Products Have Increased Rates of Clinical Trial Success throughout the Drug Development Process. 2024. 87(7): p. 1844-1851.

13. Domingo-Fernández, D., et al., Modern drug discovery using ethnobotany: a large-scale cross-cultural analysis of traditional medicine reveals common therapeutic uses. 2023. 26(9).
14. Chen, L., et al., From laptop to benchtop to bedside: structure-based drug design on protein targets. Current pharmaceutical design, 2012. 18(9): p. 1217-1239.
15. Billur Engin, H., et al., Network-based strategies can help mono-and poly-pharmacology drug discovery: a systems biology view. Current pharmaceutical design, 2014. 20(8): p. 1201-1207.
16. Bennett, J.E., R. Dolin, and M.J. Blaser, Mandell, Douglas, and Bennett's principles and practice of infectious diseases. 2014: Elsevier Inc.
17. Gupta, A.K., et al., The pathogenicity and virulence of Leishmania-interplay of virulence factors with host defenses. Virulence, 2022. 13(1): p. 903-935.
18. Chang, C.Y., et al., Gabapentin in acute postoperative pain management. 2014. 2014(1): p. 631756.
19. Jamal, Q., et al., Prevalence and comparative analysis of cutaneous leishmaniasis in Dargai Region in Pakistan. 2013. 45(2).
20. Ullah, N., et al., Plants as antileishmanial agents: current scenario. 2016. 30(12): p. 1905-1925.
21. Elawad, M.A., et al., Natural products derived steroids as potential anti-leishmanial agents; disease prevalence, underlying mechanisms and future perspectives. 2023. 193: p. 109196.
22. Kim, S., Exploring chemical information in PubChem. Current protocols, 2021. 1(8): p. e217.
23. Ru, J., et al., TCMSP: a database of systems pharmacology for drug discovery from herbal medicines. Journal of cheminformatics, 2014. 6: p. 1-6.
24. Filimonov, D., et al., Prediction of the biological activity spectra of organic compounds using the PASS online web resource. Chemistry of Heterocyclic Compounds, 2014. 50: p. 444-457.
25. Lipinski, C.A., et al., Experimental and computational approaches to estimate solubility and permeability in drug discovery and development settings. Advanced drug delivery reviews, 1997. 23(1-3): p. 3-25.
26. Husain, A., et al., Synthesis, molecular properties, toxicity and biological evaluation of some new substituted imidazolidine derivatives in search of potent anti-inflammatory agents. Saudi Pharmaceutical Journal, 2016. 24(1): p. 104-114.
27. Pires, D.E., T.L. Blundell, and D.B. Ascher, pkCSM: predicting small-molecule pharmacokinetic and toxicity properties using graph-based signatures. Journal of medicinal chemistry, 2015. 58(9): p. 4066-4072.
28. Lohohola, P.O., et al., In silico ADME/T properties of quinine derivatives using SwissADME and pkCSM webservers. 2021. 42(11): p. 1-12.
29. Banerjee, P., et al., ProTox 3.0: a webserver for the prediction of toxicity of chemicals. 2024: p. gkae303.
30. Rocha, E.C.M.d., et al., High-Throughput Molecular Modeling and Evaluation of the Anti-Inflammatory Potential of Açaí Constituents against NLRP3 Inflammasome. 2024. 25(15): p. 8112.
31. Lagunin, A.A., et al., CLC-Pred: A freely available web-service for in silico prediction of human cell line cytotoxicity for drug-like compounds. 2018. 13(1): p. e0191838.
32. Šícho, M., et al., FAME 3: predicting the sites of metabolism in synthetic compounds and natural products for phase 1 and phase 2 metabolic enzymes. Journal of chemical information and modeling, 2019. 59(8): p. 3400-3412.
33. Stork, C., et al., NERDD: a web portal providing access to in silico tools for drug discovery. Bioinformatics, 2020. 36(4): p. 1291-1292.
34. Braga, R.C., et al., Pred-hERG: A novel web-accessible computational tool for predicting cardiac toxicity. Molecular informatics, 2015. 34(10): p. 698-701.
35. Borba, J.V., et al., Pred-skin: a web portal for accurate prediction of human skin sensitizers. 2020. 34(2): p. 258-267.
36. Kolšek, K., et al., Endocrine Disruptome • An Open Source Prediction Tool for Assessing Endocrine Disruption Potential through Nuclear Receptor Binding. 2014, ACS Publications.
37. Ali, F., et al., Reprofiling analysis of FDA approved drugs with upregulated differential expression genes found in hypertension. Informatics in Medicine Unlocked, 2022. 29: p. 100895.
38. Ullah, I., Z.K. Shinwari, and A.T.J.P.J.B. Khalil, Investigation of the cytotoxic and antileishmanial effects of Fagonia indica L. extract and extract mediated silver nanoparticles (AgNPs). 2017. 49(4): p. 1561-1568.
39. Takahashi, I., et al., Purification and characterization of dimethylallyl pyrophosphate: aspulvinone dimethylallyltransferase from Aspergillus terreus. Biochemistry, 1978. 17(13): p. 2696-2702.
40. Zhang, L.-H., et al., Polyketide butenolide, diphenyl ether, and benzophenone derivatives from the fungus Aspergillus flavipes PJ03-11. Bioorganic & medicinal chemistry letters, 2016. 26(2): p. 346-350.
41. Molowa, D., A. Shayne, and P. Guzelian, Purification and characterization of chlordecone reductase from human liver. Journal of Biological Chemistry, 1986. 261(27): p. 12624-12627.
42. Bonel-Pérez, G.C., et al., Antiproliferative and pro-apoptotic effect of uvaol in human hepatocarcinoma HepG2 cells by affecting G0/G1 cell cycle arrest, ROS production and AKT/PI3K signaling pathway. Molecules, 2020. 25(18): p. 4254.
43. Lynch, T. and A. Price, The effect of cytochrome P450 metabolism on drug response, interactions, and adverse effects. American family physician, 2007. 76(3): p. 391-396.
44. de Bruyn Kops, C., et al., GLORY: generator of the structures of likely cytochrome P450 metabolites based on predicted sites of metabolism. Frontiers in chemistry, 2019. 7: p. 402.
45. De Coster, S. and N. Van Larebeke, Endocrine-disrupting chemicals: associated disorders and mechanisms of action. Journal of environmental and public health, 2012. 2012.
46. Nielsen, E., G. Ostergaard, and J.C. Larsen, Toxicological risk assessment of chemicals: A practical guide. 2008: CRC Press.
47. Sharma, S.V., D.A. Haber, and J. Settleman, Cell line-based platforms to evaluate the therapeutic efficacy of candidate anticancer agents. Nature reviews cancer, 2010. 10(4): p. 241-253.
48. Borba, J.V., et al., Pred-skin: a web portal for accurate prediction of human skin sensitizers. Chemical Research in Toxicology, 2020. 34(2): p. 258-267.
49. Chen, D., et al., Regulation of protein-ligand binding affinity by hydrogen bond pairing. 2016. 2(3): p. e1501240.

50. Dhorajiwala, T.M., et al., Computer-aided docking studies of phytochemicals from plants Salix subserrata and Onion as inhibitors of glycoprotein G of rabies virus. 2019. 3(4): p. 269-276.
51. Siddiqui, S., et al., Kaneric acid, a new triterpene from the leaves of Nerium oleander. Journal of Natural Products, 1986. 49(6): p. 1086-1090.
52. Babalola, I.T. and E.A. Adelakun, Isolation and Characterization of Two Ursane-Skeleton Triterpenoids from Eucalyptus grandis (Myrtaceae). 2017.
53. Du, S.-y., et al., Anti-inflammatory properties of uvaol on DSS-induced colitis and LPS-stimulated macrophages. Chinese Medicine, 2020. 15(1): p. 1-13.
54. Lafi, O., et al., Synergistic antileishmanial activity of erythrodiol, uvaol, and oleanolic acid isolated from olive leaves of cv. Chemlali. 3 Biotech, 2023. 13(12): p. 395.
55. Saudagar, P. and V.K. Dubey, Cloning, expression, characterization and inhibition studies on trypanothione synthetase, a drug target enzyme, from Leishmania donovani. 2011.
56. da Silva Filho, A., et al., In vitro antileishmanial, antiplasmodial and cytotoxic activities of phenolics and triterpenoids from Baccharis dracunculifolia DC (Asteraceae). Fitoterapia, 2009. 80(8): p. 478-482.